MULLARD LIMITED
Mullard House
Torrington Place
London, W.C.1

CONTENTS

Channel multiplier plates for imaging applications 210–216

Pincushion correction and convergence for 625-line colour receivers 217–222

Magnetic units in SI 223–225

D.C. amplifier to drive an electrolytic ampere-hour meter 226–228

VOL. 10 No. 97 JANUARY 1969

Mullard Technical Communications

VOLUME 10 NUMBER 97

January 1969

Mullard Technical Communications

VOLUME 10 NUMBER 97 January 1969

Contents

Channel Multiplier Plates for Imaging Applications
A. Guest, R. T. Holmshaw, and B. W. Manley 210

Pincushion Correction and Convergence for 625-line Colour Receivers
D. J. King and E. C. Thomson 217

Magnetic Units in SI *M. J. Rose* 223

D.C. Amplifier to Drive an Electrolytic Ampere-hour meter
R. S. Babbs 226

Mullard Technical Communications records new developments in the application of electronics in science, industry, and the home. It contains information on the properties and performance of discrete and integrated semiconductor devices, electronic valves and tubes, and associated magnetic, electrical, electron-optical, and electromechanical components and assemblies. The practical circuits given are, in general, designed to provide the best working conditions and most favourable performances for the devices used. Where design principles are discussed, these may be used (so far as device ratings allow) for adaptation of the published designs to meet particular requirements. Current data sheets should always be consulted before any circuit or adaptation is considered for production.

All information is published in good faith, but no guarantee of performance is given or implied. Nor does publication imply any authority or licence for the utilisation of any patented feature.

Of the devices or assemblies included in circuits, Mullard Limited can normally supply only those listed in the Company's current catalogues. Availability in large quantities should be confirmed with Mullard Limited.

Technical enquiries should be addressed to the Editor, not to the authors or laboratories named.

Six issues are published each year. Circulation (free of charge) is limited to equipment designers, research organisations, laboratories, libraries, educational establishments, and engineering consultants. Requests for addition to the mailing list must be made on the official stationery of the establishment concerned.

Abstracts, or references to an article, should mention both the source, *Mullard Technical Communications*, and the authors. Requests for republication or translation should be made to the Editor in writing. All articles in *Mullard Technical Communications* are indexed in *British Technology Index*. Abstracts appear in *Current Papers in Physics, Electrotechnology, and Control.*

'Mullard' is the trade mark of Mullard Limited and is registered in most of the principal countries of the world.

Editor: F. A. Sowan Assistant Editors: E. G. Evans A. Perry
Central Technical Services
Mullard Limited, Mullard House, Torrington Place, London, W.C.1
Telephone: 01-580 6633 Telex: 264341

© Mullard Limited, 1969

Made and Printed in England by
WIGHTMAN AND COMPANY LIMITED, 1/3 BRIXTON ROAD, LONDON, S.W.9

Channel Multiplier Plates for Imaging Applications

A. GUEST, R. T. HOLMSHAW and B. W. MANLEY
Mullard Research Laboratories

Single-channel electron multipliers have been used for some time in space exploration for the detection of low-energy electrons. This article deals with the exploitation of the device to produce two-dimensional arrays of multipliers which offer great possibilities in image detection and intensification.

INTRODUCTION

The channel electron multiplier (Refs. 1, 2, 3) is a distributed dynode multiplier which combines the functions of the dynode structure of the conventional photomultiplier and the resistor chain which divides the potential among the separate dynodes. It consists of a glass tube (Fig. 1) with a length of about fifty diameters: the inside surface is coated with a semi-insulating layer with a resistance between the electrodes at each end of the tube in the range 10^8 to $10^{14}\Omega$, depending upon the current output to be drawn from the channel.

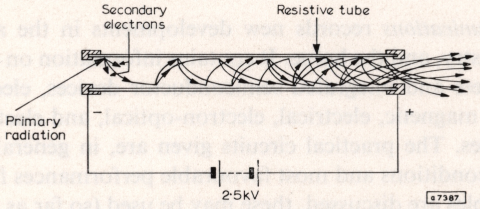

Fig. 1—Channel electron multiplier

The multiplier operates in vacuum with a potential applied between the electrodes. Electrons enter the low-potential end and strike the wall to produce secondary electrons which are accelerated axially by the applied electric field. Their transverse energy of emission causes them to traverse the channel, so that they in turn strike the wall after gaining considerable energy and produce further secondary electrons. This process is repeated many times along the channel, and many electrons emerge from the high-potential end. The gain depends upon the applied potential and upon the ratio of length to diameter of the channel, as well as on the secondary emission characteristics of the channel wall. With 1kV applied, the current gain will typically be a few thousand, while at 3kV, the gain may reach 10^8.

Since the gain does not depend upon the absolute size of the channel, the dimensions may be scaled without affecting the performance, and honeycomb arrays of parallel channel multipliers, called channel plates, may be constructed (Ref. 4).

Since the channels are usually made from special glasses which may be made electronically conducting, the techniques for the manufacture of channel plates may be similar to those used for fibre optics (Refs. 5, 6).

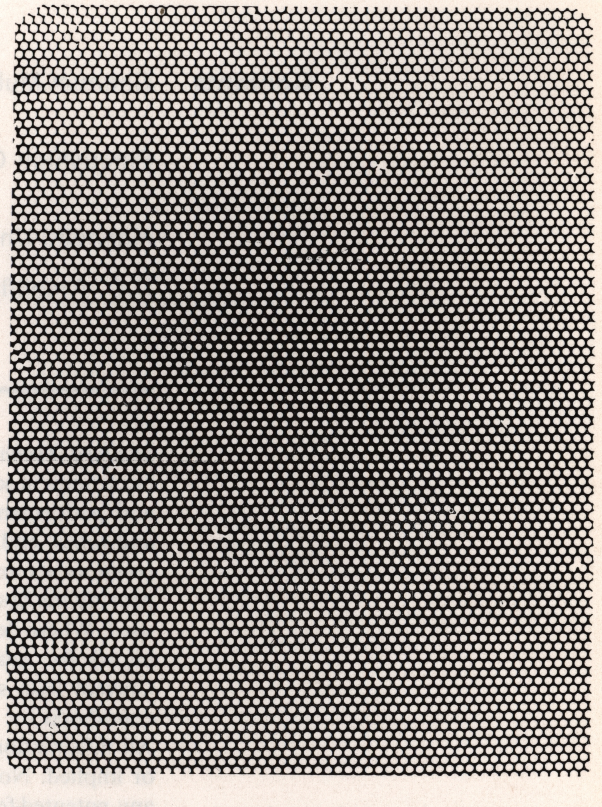

Fig. 2—Microscope view of part of channel plate composed of 40μm diameter channels

Tubing is drawn down to the required diameter either in one drawing operation, or in two stages in which many channels of an intermediate diameter are assembled and the bundle of channels drawn until the constituent channels are of the right diameter. These multiple units are then arranged together to make up the required area. The total bundle is sliced and polished into discs to give the necessary ratio of channel length to diameter.

The separate multipliers are connected in parallel by evaporating at an oblique angle a thin metallic coating of Nichrome over the two polished surfaces of the plate. The film connects the interstices of the channels but leaves the channels open. Electrical connection is made to the channels by a peripheral ring electrode pressed against each face of the plate. Fig. 2 shows a microscope view of part of a plate composed of 40μm diameter channels. The thickness of the plate is 2·4mm and the open area is 62%.

COMPUTER MODEL OF CHANNEL PLATE

To assist in the analysis of channel plate performance, a computer model has been produced, which when taken in conjunction with experimental results, allows some measure of generalisation to be applied to the data.

The present model is designed to minimise the number of simplifying assumptions and to include as much experimental evidence as possible within its structure. Although a gain limiting process is observed in practical multipliers when the gain is very high (Refs. 3, 7, 8) this model applies only to a channel operated in conditions in which space charge and wall charging do not modify significantly the channel performance. No evidence has been seen of space charge effects at gains below 10^6; thus the model is applicable to most imaging applications, where electron gains in excess of 10^5 are seldom required.

A random number generating procedure is used in the computer programme to calculate the result of a primary electron collision with the channel wall.

The mean yield, δ, as a function of electron energy in eV and angle of incidence θ is described by the function derived in the Appendix (page 215):

$$\delta' = (V'\surd\cos\theta)^{\beta}\exp[\alpha(1-\cos\theta)+\beta(1-V'\surd\cos\theta)]$$

where δ' and V' are normalised to the maximum value of δ at normal incidence, and β is a constant which controls the form of the expression. Whenever a collision is simulated, the appropriate form of the secondary emission function is used to determine the mean yield of electrons from the particular impact energy and angle of inclination. This value is used as the mean of a Poisson distribution, and the actual number of secondaries generated by the collision is a random sample chosen from the distribution. Similarly, the emission angles are chosen from a cosine distribution and the energies from a Rayleigh distribution with a modal energy which may be controlled in the programme. The trajectory of each secondary electron produced in this way is calculated from the ballistic equations; so the position, energy, and angle of the subsequent collision with the channel wall are determined in three dimensions. The result of each collision is calculated as before, and the process is repeated for every secondary electron generated. The length of channel available to each secondary for multiplication is stored in the computer, and this information is updated at every collision. The total number of electrons which have left the output of the channel is accumulated continually, so that when all the electrons are calculated to have emerged from the channel, the total yield is known. The process is repeated for many individual initiating electrons to produce a series of output pulses.

By keeping the energy of the input electrons and the secondary electron characteristics constant for a complete set of output pulses, the effects of independent variation of the applied voltage and the length-to-diameter ratio on the following properties can be studied:

1) The mean gain G and the variance σ can be derived directly from the series of pulses.

2) The noise factor F, which can be expressed

$$F = \left[\frac{\text{Input signal to noise ratio}}{\text{Output signal to noise ratio}}\right]^2 = 1 + \frac{\sigma^2}{G^2}$$

can be derived.

3) If sufficient pulses are obtained for one set of conditions it is possible to plot a pulse amplitude distribution indicating the relative frequency of output pulses of a particular size.

In addition, it is possible to study the effect of the primary electron energy, and of variations in the secondary emission characteristics of the first collision, on the behaviour of a channel multiplier.

It is also possible to determine the energy and directional distribution of the electrons leaving the end of the channel.

The approximate values of the parameter which control the form of the secondary emission function in the programme can be deduced from published experimental results (Refs. 9, 10, 11). It has been found that different channels of the same material behave in a slightly different fashion; this variation may result from small differences in the processing of the material, or in the operational environment. To determine precisely the parameters appropriate for the simulation of a practical channel, it is necessary to calibrate the programme with a typical set of experimental results; for example, the gain of the channel with a specific applied voltage, length-to-diameter ratio, and controlled input conditions. The form parameters of the secondary emission characteristic must then be adjusted until the results from the computer agree with the experimental values. It is then possible to simulate various operating conditions with the secondary emission parameters set to the constant calibrated values.

Conversely, the effects of variations in the form of the secondary emission function with constant operating conditions can be simulated.

Extensions of this programme permit the transit time and transit time spread to be determined, but at present no experimental evidence is available to compare with the computer results.

PERFORMANCE OF CHANNEL PLATES

Measurements on plates composed of 40μm diameter channels have been made in sealed-off envelopes containing S20 type photocathodes. This has made possible relatively simple control and measurement of low input currents, and precise control of the input energy of electrons to the channel plate. For measurements of noise factor and pulse amplitude distribution, experimental image intensifiers were used, and the channel plate output was monitored with a photomultiplier.

Gain

The measured current gain of a channel plate composed of 40μm diameter channels, with a length-to-diameter ratio, γ, of 60 is shown as a function of voltage in Fig. 3.

The gain from a channel plate will depend upon the value of γ, so it is necessary to consider what factors

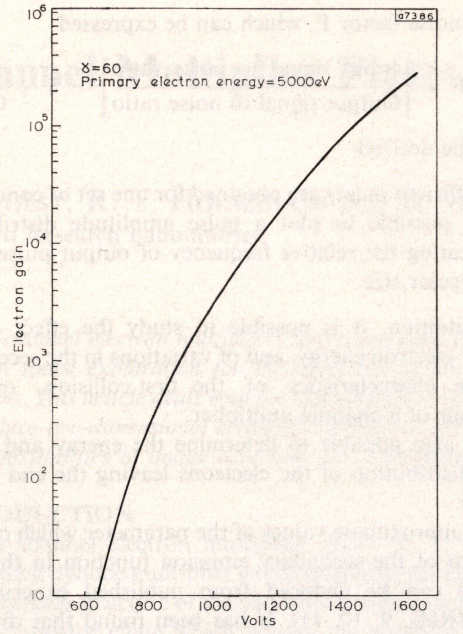

Fig. 3—Gain as a function of voltage with γ constant

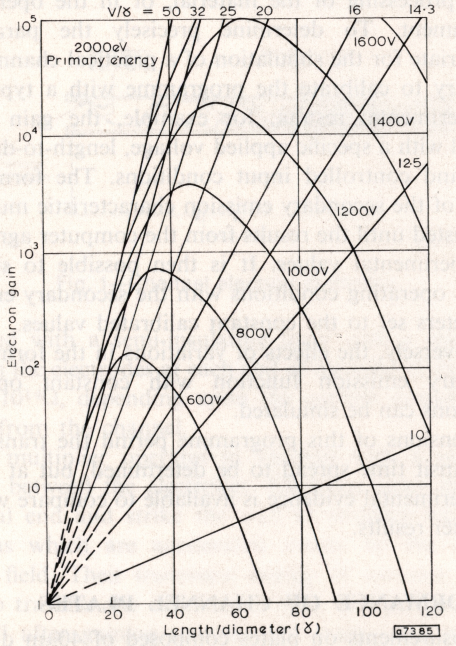

Fig. 4—Universal gain curve for channel

influence the choice of this parameter. By using the measured gain of Fig. 3 to calibrate the computer model, a universal gain curve can be derived (Fig. 4), from which it can be seen that at a constant voltage there is a region in which the gain varies least with variations in γ. This is a desirable operating point since (1) the gain is a maximum at a particular applied voltage, and (2) the gain variation from channel to channel will be least dependent on differences in channel diameter. The optimum value of γ occurs when the applied potential is approximately 22γ volts. Thus as the voltage applied to the plate is changed, the operating point will depart from the optimum. The value of γ = 60 was chosen as a suitable compromise within the likely range of gain required for imaging applications.

The gain measurements were made at an input current of 10^{-12}A. The maximum output current from the plate was thus substantially less than the conduction current in the plate, determined by its resistance of $10^9\Omega$. The saturation effect of drawing output currents approaching the value of the conduction current may be seen from the current transfer characteristics (Fig. 5). The operation of the channel plate is linear for output currents less than 5% of the conduction current.

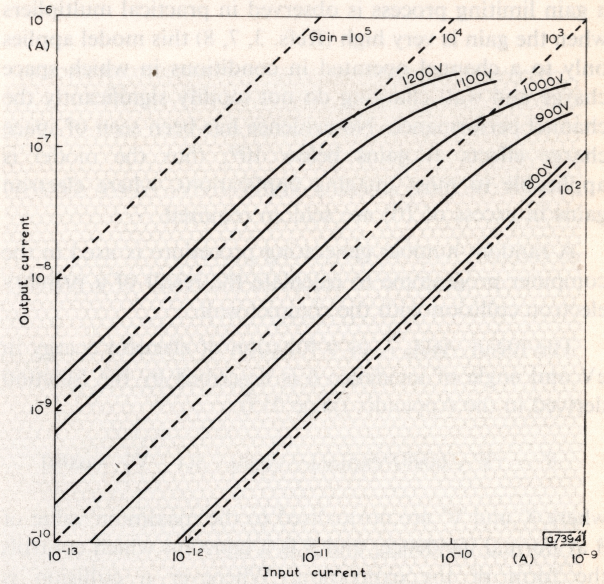

Fig. 5—Current transfer characteristics of a channel plate

The measured gain values were used to calibrate the computer model in all subsequent simulations of the noise factor of the channel plate.

Noise Factor

The noise factor of a channel plate is a measure of the information loss resulting from its use.

The measured value of the noise factor depends upon the input energy of the primary electrons, and upon the potential applied to the plate. The optimum value is typically about 4.

The information loss is due to a number of factors:

1) Loss of electrons at the input of the plate, the open area of which is about 60%.

2) A loss when primary electrons fail to produce secondary electrons, or secondary electron cascades die out after a few stages.

3) The variation in gain among the output electron pulses resulting from the statistical variation of the secondary emission yield.

The noise factor has been measured by incorporating the channel plate in an experimental image intensifier, and observing the signal-to-noise ratio on the fluorescent screen with a photomultiplier and an r.m.s. voltmeter having a variable integration time. With increasing integration time, the noise factor increases to an asymptotic value where it is unaffected by the phosphor decay time (Fig. 6).

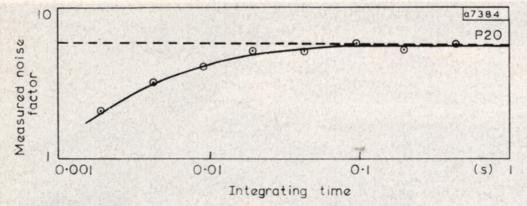

Fig. 6—Measured noise factor as a function of voltmeter integrating time (P20 (KA) phosphor)

The asymptotic value of noise factor has been measured as a function of input electron energy; these values are compared with the computer simulation results in Fig. 7. This variation in noise factor results from the change in secondary emission yield with the energy of the primary electrons. The optimum is not well defined but occurs around 1000eV.

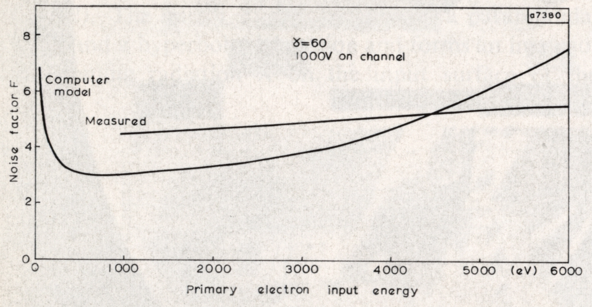

Fig. 7—Asymptotic value of noise factor as a function of input electron energy

The noise factor is shown as a function of channel plate voltage in Fig. 8. The high noise factor at low voltages results from the low energy gained by electrons between collisions and consequently the significant probability of zero secondary emission yield in the early stages of pulse build-up.

A principal factor contributing to the loss in information is the variation in output electron pulse amplitude from pulse to pulse—the pulse height distribution.

Pulse Height Distribution

The pulse height distribution has proved difficult to measure directly because of the problem of detecting the very small pulses in the distribution. Measurements in an experimental image intensifier incorporating a P16 phosphor have been made by observing the output with a photomultiplier and recording the pulse height distribution on a multichannel analyser. The results follow a negative exponential form down to very low values of output pulse height. Inaccuracies in the measurements at these values are due to the still significant decay of the P16 phosphor causing spurious pulses to be recorded by the analyser during the decay period. Fig. 9 shows the experimental results compared with a computer-simulated histogram of pulse heights.

It should be noted that the negative exponential distribution produced in the simulation results from the presumption of Poisson distribution of secondary emission yield about the mean, but a mean which varies according to the collision energy and angle.

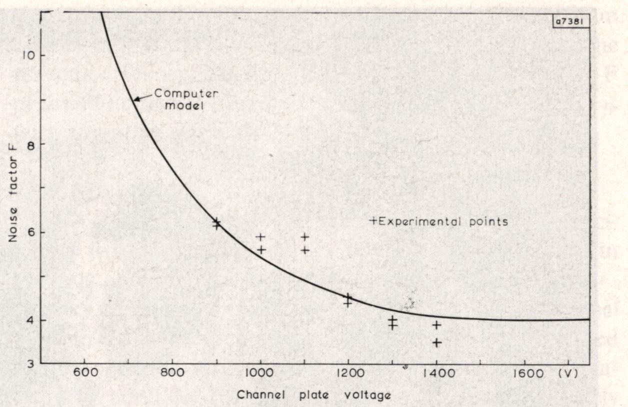

Fig. 8—Noise factor as a function of channel plate voltage

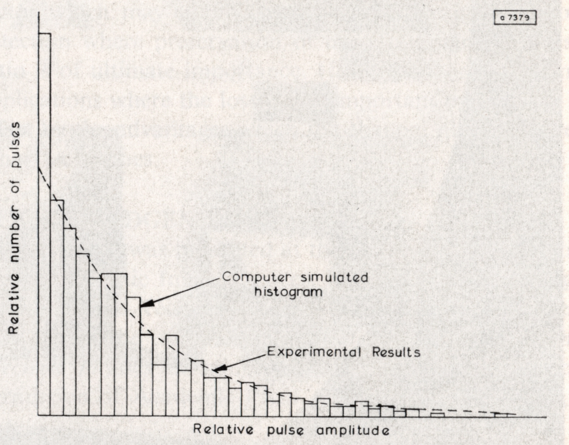

Fig. 9—Example of pulse height distribution, with experimental results shown by the broken line

The occurrence of a pulse height distribution of negative exponential form may be shown to be consistent with the measured noise factors. The measured fluctuation in the output signal from a channel plate results from the contribution of the input signal fluctuation and the added statistical fluctuation introduced by the secondary emission in the channel plate. Presuming the rate of arrival of input electrons at the plate to fluctuate about the mean n according to a Poisson distribution, the r.m.s. deviation from the mean will be $n^{\frac{1}{2}}$, which is the input noise N_i. This will result in an r.m.s. deviation at the output of $n^{\frac{1}{2}}G$ where G is the mean gain of the plate.

The gain process will result in a yield for each input electron distributed about the mean with a standard deviation σ. The total variance for a sequence of n electrons will be $n\sigma^2$, the sum of the variance for each. Hence the r.m.s. deviation introduced by the channel plate at the output is $n^{\frac{1}{2}}\sigma$.

If the two noise contributions are uncorrelated we may add them in quadrature to obtain the total r.m.s. deviation, which is the measured noise, N_o:

$$N_o = (nG^2 + n\sigma^2)^{\frac{1}{2}}.$$

The negative exponential pulse height distribution may be described by a Furry distribution (Ref. 12) for which

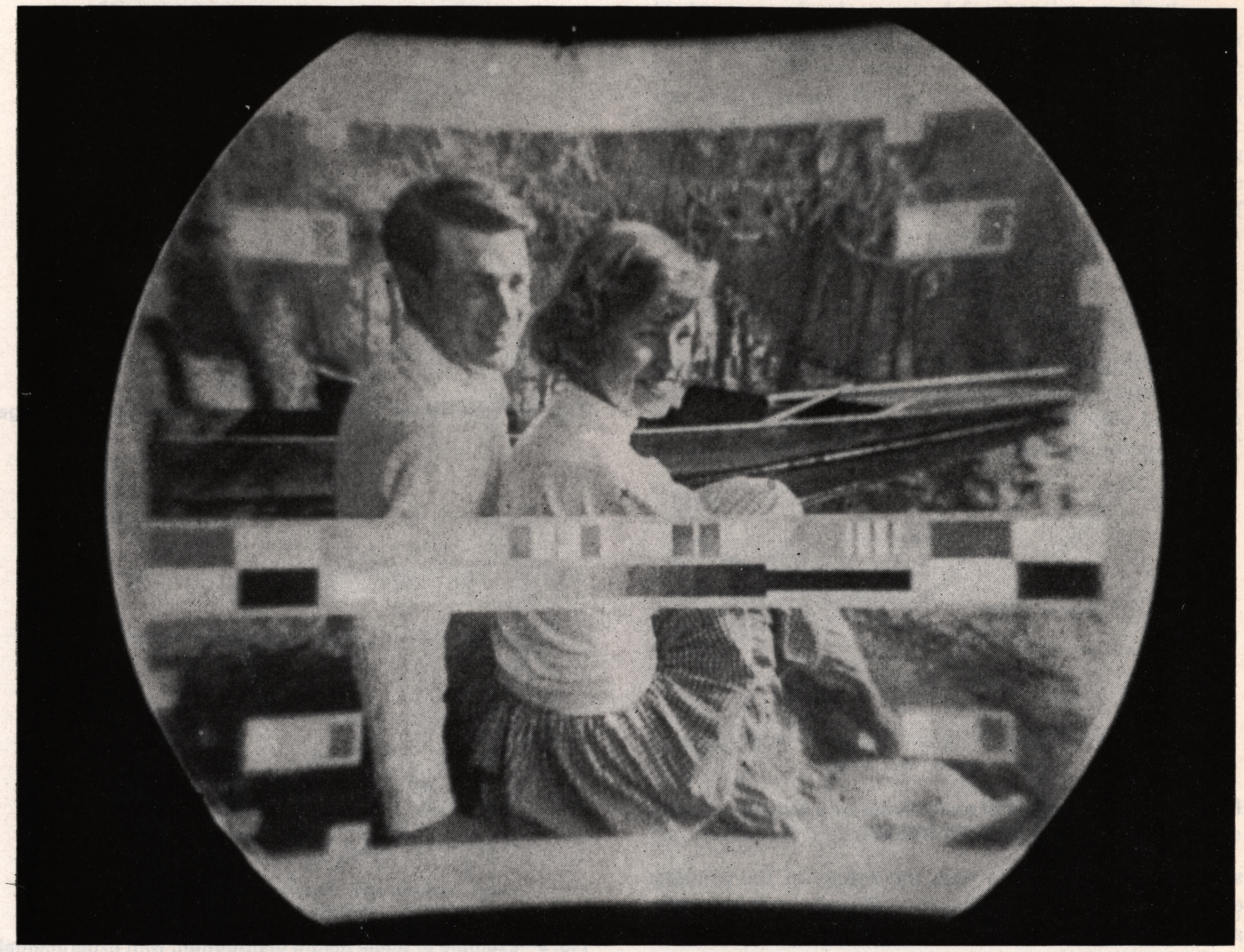

Fig. 10—Image from screen of experimental image intensifier with channel plate composed of 40μm diameter channels

the variance is given by:

$$\sigma^2 = G(1+G)$$

hence

$$N_o = n^{\frac{1}{2}}(2G^2+G)^{\frac{1}{2}}.$$

Since G is large, this reduces to:

$$N_o = (2n)^{\frac{1}{2}}G.$$

The noise factor of the channel plate may be written:

$$F = \left\{\frac{N_o}{GN_i}\right\}^2$$

from which we find the noise factor for the channel plate to be 2.

Because the channel plate open area is about 60%, the noise factor becomes 3·3, and this will be further increased in proportion to any loss of electrons at the first collision, and by any channel-to-channel non-uniformity in performance. This latter spatial noise will depend very largely upon the dimensional accuracy with which the channels are fabricated.

Channel Plate Uniformity

By controlling the diameter of the separate channels within about 5%, uniform operation can be obtained over the area of the plate. This is demonstrated by the photograph (Fig. 10) taken from the screen of an experimental image intensifier containing a channel plate composed of 40μm channels.

APPLICATION OF CHANNEL PLATES

Channel plates are physically rugged and stable in air, so no special care need be taken with their storage. They are thus well suited to applications in electron-optical imaging systems, both in sealed-off devices, like the image intensifier described by Eschard (Ref. 13) and in demountable experiments requiring frequent exposure to air. Fig. 11 shows a diagram of an experimental X-ray image intensifier containing a channel plate. The proximity of photocathode and screen to the channel plate avoids the use of electron-optical lenses, thus offering the possibility of a compact 'panel' intensifier operating at considerably lower voltages than conventional X-ray intensifiers.

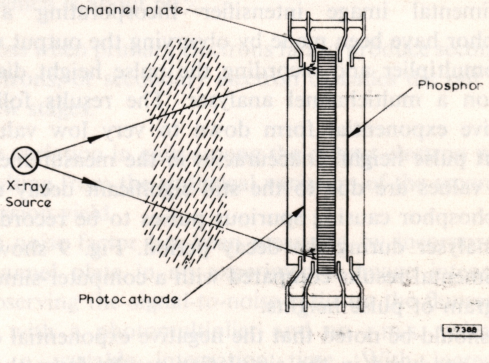

Fig. 11—Experimental X-ray image intensifier containing a channel plate

Further possibilities exist for the use of channel plates in space exploration. They will operate satisfactorily in pressures below 10^{-5} torr,* thus the environmental vacuum of space is adequate. In this way no input window is necessary, and the detection efficiency of a channel plate in the range 1 to 10nm (1240eV to 124eV) in which much stellar radiation falls, is good. By placing a channel plate at the focus of a satellite-borne X-ray telescope, and using the sensitivity of the input electrode of the plate to convert the X-rays into photo-electrons, an intensified image of the X-ray pattern can be obtained. The output electrons from the plate can be recorded on film, or they may be used to excite a phosphor viewed by a television camera tube whose output signal is transmitted to a ground station (Fig. 12), The mirror M is composed of a paraboloidal section and a hyperboloidal section and forms an image of the incoming radiation X on the input surface of the channel plate CP. The resulting electrons emerging from the output surface of the plate are accelerated to the phosphor Ph deposited on the fibre optic input window F of the Plumbicon† tube T. The electrical output signal S is telemetered to earth.

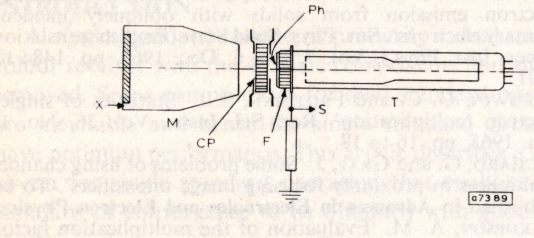

Fig. 12—Proposed soft X-ray astronomical telescope

CONCLUSIONS

The extension of the channel electron multiplier principle to two-dimensional arrays offers new possibilities in imaging applications.

Very high electron gain can be obtained from a channel plate in a compact length and at a low voltage compared to that required in other techniques of image intensification. In addition the device is air stable and relatively robust, thus lending itself to demountable use as well as in sealed-off tubes.

The loss of information in a channel plate is a significant factor which may limit its usefulness for single electron detection where preservation of the input signal-to-noise ratio is of ultimate importance. However, there are many applications where the loss is not important or where it is offset by the advantages which the channel plate has over other techniques.

ACKNOWLEDGEMENTS

This paper was presented at the Fourth Symposium on Photo-electronic Image Devices, held at Imperial College of Science and Technology, London, 16 to 20 September, 1968. It will be published in *Advances in Electronics and Electron Physics* in mid-1969, and it appears here by permission of Academic Press.

APPENDIX

The Secondary Emission Function used in the Computer Model

The function chosen to represent the secondary emission coefficient as a function of energy (V) and angle of incidence (θ) must satisfy the following results which have been determined experimentally.

a) The curve for normal incidence should be a close approximation to the published experimental curves.

b) $$V_{m(\theta)} = \frac{V_{m(0)}}{\sqrt{\cos\theta}} \qquad \ldots(1)$$

where the subscripts θ and 0 indicate the angle of incidence.

c) $$\delta_{m(\theta)} = \delta_{m(0)} \exp[\alpha(1-\cos\theta)]. \qquad \ldots(2)$$

(Refs, 14,15).

where

V_m is the collision energy in eV which is equivalent to δ_m, the maximum secondary emission yield,

and

α is a constant of the material.

Let $V' = V/V_{m(0)}$

$\delta' = \delta/\delta_{m(0)}$.

Now $\delta' = \delta'(V', \theta)$ so it is assumed that δ' may be taken as the product of two functions, one of which is a function of θ alone. That is:

$$\delta' = f(V', \theta)\,F(\theta).$$

Differentiating with respect to V′,

$$\left(\frac{\partial\delta'}{\partial V'}\right)_\theta = F(\theta)\left(\frac{\partial f}{\partial V'}\right)_\theta.$$

As the observed secondary emission curves have a single maximum, assume that a possible representation of the function f is

$f = A(V')^n \exp[-\beta V'\sqrt{\cos\theta}]$ with A, β, and n constants.

Differentiating with respect to V′,

$$\left[\frac{\partial f}{\partial V'}\right]_\theta = A\exp[-\beta V'\sqrt{\cos\theta}](nV'^{(n-1)} - \beta V'^n\sqrt{\cos\theta}) \qquad \ldots(3)$$

at V'_m, $V'_m = n/(\beta\sqrt{\cos\theta})$.

So that to satisfy Eq. 1,

$$n = \beta \qquad \ldots(4)$$

and $$\delta' = AV'^\beta \exp[-\beta V'\sqrt{\cos\theta}]F(\theta). \qquad \ldots(5)$$

At the maximum, from Eq. 2:

$$\delta'_m = A\left(\frac{1}{\sqrt{\cos\theta}}\right)^\beta \exp(-\beta)F(\theta) \equiv \exp[\alpha(1-\cos\theta)], \qquad \ldots(6)$$

so that $$F(\theta) = \exp[\alpha(1-\cos\theta)+\beta].(\sqrt{\cos\theta})^\beta/A \qquad \ldots(7)$$

and

$$\delta' = (V'\sqrt{\cos\theta})^\beta \exp[\alpha(1-\cos\theta)+\beta(1-V'\sqrt{\cos\theta})]. \qquad \ldots(8)$$

---

*1 torr = 133·322 N/m²

†'Plumbicon' is the registered trademark for tv camera tubes

The value of β is chosen to fit the published secondary emission curves at normal incidence. Unfortunately, it was not possible to match the curve over its entire range with the same value of β.

For $V' \leqslant 1$, β lies in the region of $0\cdot55$ to $0\cdot65$.
For $V' \geqslant 1$, β is approximately $0\cdot25$.

The two forms of the function are approximately equal when $V' = 1\cdot5$.

The value of the constant α has been determined by experiment (Ref. 10), and the value $\alpha = 0\cdot62$ was used in the programme. It must be understood that the particular form of the function used to simulate the secondary emission characteristics was chosen because its shape was similar to the experimental curves.

The gain of the channel is determined by the precise value of the low-energy constant β. This constant was varied within the region stated above, and the value which best simulated an actual gain measurement was chosen. As the gains of several channels may differ because of slight variations in the manufacturing process, the value of β can be varied slightly to give the best fit for each case. One value of the low-energy β has been used in all the simulations described in this article, and this has been adequate for the simulations described.

REFERENCES

1. Wiley, W. C. and Hendee, C. F. 'Electron multipliers utilising continuous strip surfaces'. **IRE Trans. Nuclear Science,** Vol. NS-9, No. 3, June 1962, pp103 to 106.
2. Adams, J. and Manley, B. W. 'The channel electron multiplier'. **Electronic Engineering,** Vol. 37, No. 445, March 1965, pp. 180 to 181.
3. Adams, J. and Manley, B. W. 'The mechanism of channel electron multiplication'. **IEEE Trans. Nuclear Science,** Vol. NS-13, No. 3, June 1966, pp. 88 to 99.
4. Adams, J. and Manley, B. W. 'The channel electron multiplier, a new radiation detector'. **Philips Tech. Rev.,** Vol. 28, No. 5/6/7, 1967, pp. 156 to 161 (available from Mullard Ltd as reprint TP995).
5. Kapany, N. S. 'Fiber optics: principles and applications'. Academic Press, New York, 1967.
6. Mullard Ltd. 'Improvements in or relating to image intensifiers' British Patent 1 064 072 (1963).
7. Evans, D. S. 'Low energy charged-particle detection using the continuous-channel electron multiplier' **Rev. Sci. Instr.,** Vol. 36, No. 3, March 1965, pp. 375 to 382.
8. Schmidt, K. C. and Hendee, C. F. 'Continuous channel electron multiplier operated in the pulse saturated mode'. **IEEE Trans. Nuclear Science.** Vol. NS-13, No. 3, June 1966, pp. 100 to 111.
9. Hachenberg, O. and Brauer, W. 'Secondary electron emission from solids'. **Advances in Electronics and Electron Physics,** Vol. XI, 1959, pp. 413 to 499.
10. Chuiko, G. A. and Yakobson, A. M. 'The fundamental characteristics of high lead content glasses as material for a continuous dynode secondary electron multiplier'. **Radio Engineering and Electronic Physics,** Vol. 11, No. 9, Sept. 1966, pp. 1471 to 1475.
11. Bronshtein, I. M. and Denisov, S. S. 'Study of secondary electron emission from solids with obliquely incident primary electrons'. **Sov. Phys. Solid State** (English translation Amer. Inst. Phys.), Vol. 7, No. 6, Dec. 1965, pp. 1484 to 1491.
12. Baldwin, G. C. and Friedman, S. I. 'Statistics of single-electron multiplication'. **Rev. Sci. Instr.,** Vol. 36, No. 1, Jan. 1965, pp. 16 to 18.
13. Eschard, G. and Graf, J. 'Some problems of using channel multipliers in proximity focusing image intensifiers'. To be published in **Advances in Electronics and Electron Physics.**
14. Yakobson, A. M. 'Evaluation of the multiplication factor of a secondary-electron multiplier (multidyne) with a continuous dynode'. **Radio Engineering and Electronic Physics,** Vol. 11 No. 10, Oct. 1966, pp. 1590 to 1600.
15. Bruining, H. 'Physics and applications of secondary electron emission'. Pergamon Press, 1954.

Pincushion Correction and Convergence for 625-line Colour Receivers

D. J. King and E. C. Thomson
Mullard Central Application Laboratory

Line convergence and pincushion correction circuits designed for optimum performance in single standard 625-line colour receivers are described. Two field convergence circuits are shown. One is for use with a field timebase which employs a valve and transformer in the output stages. A second circuit is described for use with transformerless single-ended push-pull output stages.

INTRODUCTION

A single standard receiver is primarily a dual standard colour receiver with the 405-line components and switches removed. Some compromises for dual standard operation are inevitable and hence the single standard circuit can have optimum performance. This article describes a simple circuit for single standard operation that enables a high standard of convergence to be obtained with good raster shape.

PINCUSHION CORRECTION

When the 90° shadow-mask colour picture tube and its associated components were developed it was found that a degree of pincushion distortion was inevitable when the deflection coils were designed for optimum spot quality. The typical amount of this distortion is some 3% N-S* and about 2·3% E-W. It is generally considered that this level of distortion is unacceptable.

Since in colour television receivers good spot quality is of major importance, the deflector coil design must not be compromised. Therefore some external means of pincushion correction is required. This external correction must take place about the centre of deflection if purity and convergence are not to be disturbed. Pincushion correction must therefore be applied dynamically, and may be achieved by modulating the line deflection current with a parabola waveform at the field frequency to correct the E-W distortion, and the field deflection with parabola at line frequency for N-S correction.

The effect of this modulation on a pincushion raster is shown in Fig. 1, where the raster width is progressively reduced away from the centre. The N-S correction takes the form of an increase in raster height in the middle of each scanning line, the effect again being greatest at the top and bottom of the screen.

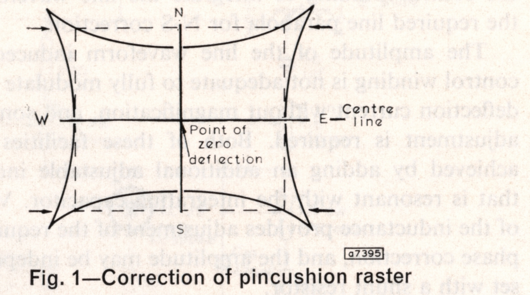

Fig. 1—Correction of pincushion raster

Simultaneous correction can be achieved by cross-modulating the scanning current in a special transductor. This consists of specially shaped Ferroxcube E cores with windings on all three limbs as shown in Fig. 2. The centre winding L_2 is used for control purposes and the two outer windings L_3 and L_4 are the controlled load impedances. Interaction between the control and load windings is minimised by connecting L_3 and L_4 in series in opposite senses. The control winding is connected in series with the field deflection coils and the magnetic field (ϕ_1) due to the vertical scanning current is shown dotted. The potentials induced across L_3 and L_4 by this flux are equal and opposite, but because of the coil configuration no potential is applied to the line deflection coils. The line scanning current causes a current to flow through L_3 and L_4 which produces a magnetic flux ϕ_2 around the outer limb (Fig. 2). When the vertical scanning current is zero there is no flux in the centre limb. As the vertical scanning current increases from zero the resulting flux interacts with the line flux, adding in one outer limb and subtracting in the other. The flux addition results in one half of the transductor being driven into saturation, and this has two effects.

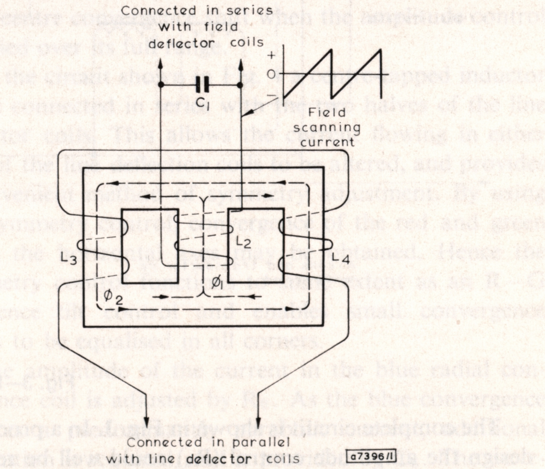
Connected in series with field deflector coils
+
0
−
C1
Field scanning current
L2
L3
L4
Ø1
Ø2
Connected in parallel with line deflector coils
a7396/1
Fig. 2—Transductor for cross-modulating the scanning current

---

*North-South refers to the vertical axis with north at the top. East-West is the horizontal axis with east on the viewer's right.

Firstly, the impedance of L_3 and L_4 falls proportionally to the vertical scanning current. These coils are connected in parallel with the line deflection coil, hence the line scan is modulated by the varying shunt load to produce the required E-W correction. The shape and magnetic properties of the transductor core cause this modulation to be approximately parabolic.

Secondly, transformer action now occurs with the unsaturated limb, and a component at line frequency appears across the control winding. Since the saturation is controlled by the vertical scanning current this component will increase with current and the phase will change, depending on saturation. A capacitor is connected across the control winding to integrate the line waveform into the required line parabola for N-S correction.

The amplitude of the line waveform induced in the control winding is not adequate to fully modulate the field deflection current without magnification, and some phase adjustment is required. Both of these facilities can be achieved by adding an additional adjustable inductance that is resonant with the integrating capacitor. Variation of the inductance provides adjustment of the required N-S phase correction, and the amplitude may be independently set with a shunt resistor.

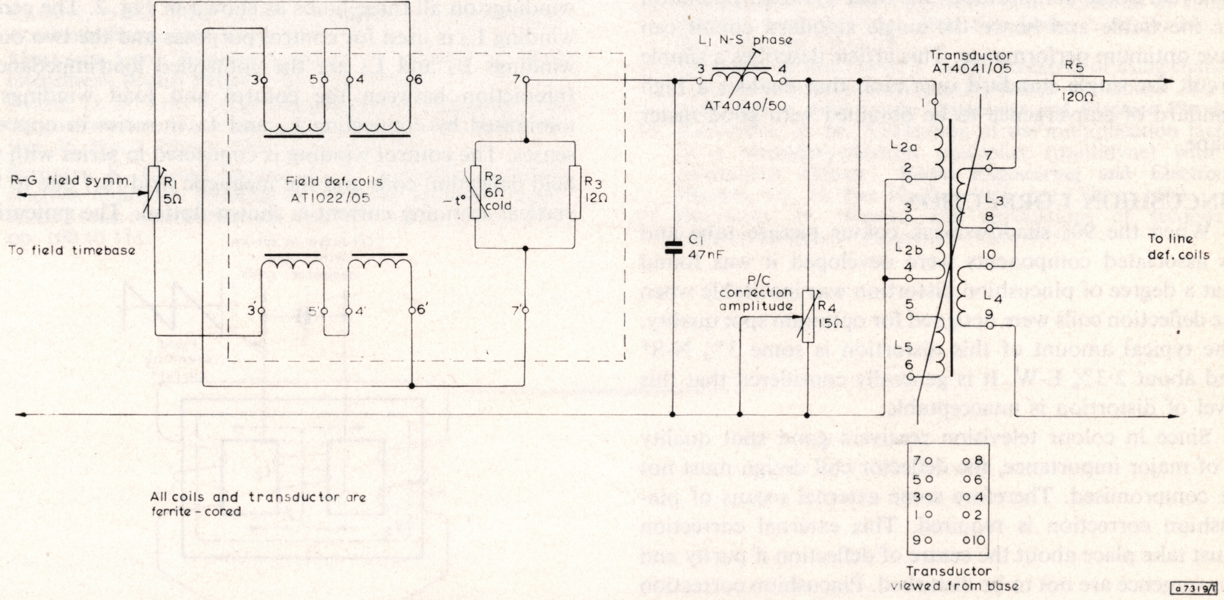
L1 N-S phase
3
4
AT4040/50
Transductor
AT4041/05
R5
120Ω
3
5
4
6
7
1
L2a
2
7
L3
8
3
L2b
4
10
L4
9
5
L5
6
R-G field symm.
R1
5Ω
Field def. coils
AT1022/05
R2
6Ω
cold
−t°
R3
12Ω
C1
47nF
P/C
correction
amplitude
R4
15Ω
To line
def. coils
To field timebase
3'
5'
4'
6'
7'
All coils and transductor are
ferrite-cored
7
8
5
6
3
4
1
2
9
10
Transductor
viewed from base
a7319/1

Fig. 3—Pincushion correction circuit

The complete circuit is shown in Fig. 3. In a production design the amplitude control (R_4) could well be replaced by a selected resistor of about 7Ω. The phase corrector coil L_1 forms part of a high Q resonant circuit and the correct tuning point is critical. The location of this inductor should be chosen carefully since stray magnetic pick-up can cause asymmetric N-S correction.

The field deflector coil interconnections also require careful consideration. The field coils consist of two separate coils, each of which is bifilar wound. Hence four different configurations and three different impedances are possible. An all-series connection, or connection in series of two pairs of coils, can give rise to line/field crosstalk which is particularly severe if the line deflector coils are not exactly balanced about an 'earthy' point. The usual way to reduce this crosstalk is to place damping resistors across each pair of field coils but these also damp the N-S correction waveform which results in insufficient correction. Therefore these configurations of coil connections should not be used. The recommended arrangement is for the bifilar coils to be connected as series pairs with the two pairs used in parallel, as shown in Fig. 3.

DYNAMIC LINE CONVERGENCE

In colour receivers employing a shadow-mask picture tube a better standard of convergence can be maintained if the line convergence is unaffected by reasonable variations of picture width and line linearity. In addition, the setting-up procedure (Ref. 1) may well be made easier since it is very difficult to adjust the width and linearity correctly before the picture is dynamically converged.

Since convergence is a function of scanning, excellent tracking of line convergence with picture width will be obtained by using the scanning current to supply the line convergence coils.

The shape of the current flowing in the line deflector coil is inherently suitable for dynamic convergence, requiring only a small amount of additional integration. Since less modification of the waveform by shaping circuits is required, a far more consistent convergence is obtained. In the circuit about to be described, the green, red, and blue radial convergence coils, and the blue lateral coils, are all connected in series with each other. The complete network is then connected in series with the line deflector coils.

However, it is normal practice to balance the deflection coils about an 'earthy' point to reduce electrostatic radiation. Therefore, a direct connection in series with either of the deflector coils' leads would result in the convergence coils being pulsed several hundred volts above chassis potential. Since this is undesirable it is preferable to connect the convergence coils into the 'cold' point (that is, the

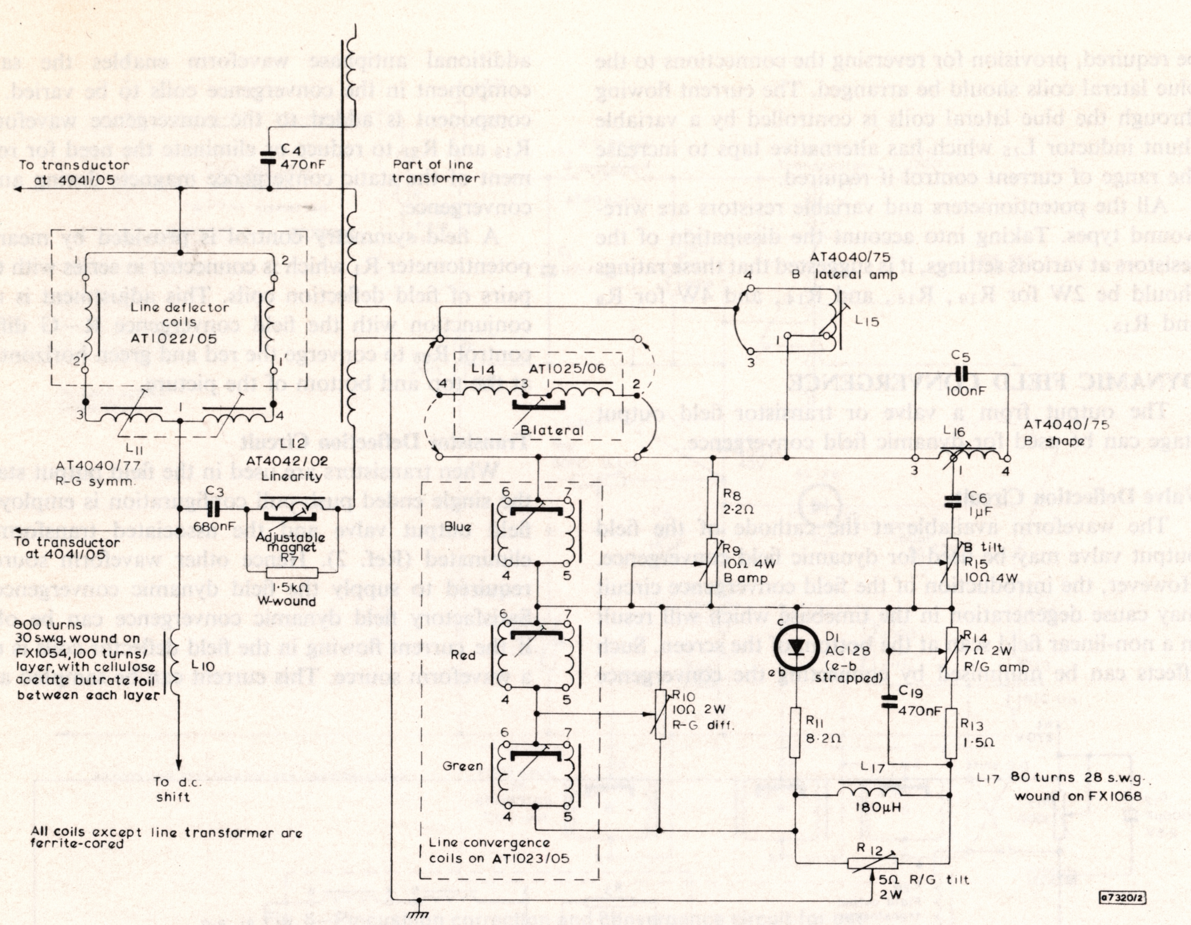
To transductor
at 4041/05
C4
470nF
Part of line
transformer
Line deflector
coils
AT1022/05
1
2
2
1
3
4
L11
AT4040/77
R-G symm.
L12
AT4042/02
Linearity
C3
680nF
Adjustable
magnet
R7
1·5kΩ
W-wound
To transductor
at 4041/05
800 turns
30 s.w.g. wound on
FX1054, 100 turns/
layer, with cellulose
acetate butrate foil
between each layer
L10
To d.c.
shift
All coils except line transformer are
ferrite-cored
L14
AT1025/06
4
3
2
Blateral
6
7
Blue
4
5
6
7
Red
4
5
6
7
Green
4
5
Line convergence
coils on AT1023/05
AT4040/75
B lateral amp
4
1
3
L15
C5
100nF
AT4040/75
B shape
L16
3
1
4
C6
1μF
R8
2·2Ω
R9
10Ω 4W
B amp
B tilt
R15
10Ω 4W
c
eb
D1
AC128
(e-b
strapped)
R14
7Ω 2W
R/G amp
R10
10Ω 2W
R-G diff.
C19
470nF
R11
8·2Ω
R13
1·5Ω
L17
180μH
L17 80 turns 28 s.w.g.
wound on FX1068
R12
5Ω R/G tilt
2W
a7320/2

Fig. 4—Single standard line convergence circuit

centre point) of the deflection coil winding on the line transformer, as shown in the complete circuit in Fig. 4. This method is satisfactory provided that the true scanning current is applied to the convergence network and no additional currents such as those flowing in the boost capacitor, e.h.t. coupling winding or the d.c. shift isolating inductor L_{10} are introduced into the convergence circuit.

The individual red, green, and blue radial convergence coils are connected in parallel pairs, and the coils on the blue lateral unit are connected in series. This forms a high current, low voltage configuration which is suitable for connecting into the line deflection circuit, which has a deflection current typically 2·8A peak-to-peak.

A variable resistor R_{14} is connected in parallel with the red and green convergence coils to adjust the amplitude of R/G convergence current. The tilt inductor L_{17} forms either a shunt or series inductance with the red and green convergence coils by adjustment of the R/G tilt control R_{12}. The sawtooth component of the R/G convergence current can be increased or decreased by adjustment of this control. A clamp diode D_1 is included in the red and green convergence circuits to eliminate the need for continual readjustment of the red and green static magnets when adjusting the R/G line dynamic convergence. Furthermore, the inclusion of the diode tends to isolate the functions of the amplitude and tilt controls and allows the effect of each to be seen more clearly on the screen. A suitable diode is an AC128 transistor with its base and emitter strapped. The value of the limiting resistor R_{11} in series with the clamp diode has been chosen so that there is no centre convergence shift when the amplitude control is varied over its full range.

In the circuit shown in Fig. 4 a centre-tapped inductor L_{11} is connected in series with the two halves of the line deflector coils. This allows the current flowing in either half of the line deflection coils to be altered, and provides a convenient method of symmetry adjustment. By using this symmetry control, convergence of the red and green along the horizontal axes may be obtained. Hence the symmetry control functions to some extent as an R−G difference tilt control and enables small convergence errors to be equalised in all corners.

The amplitude of the current in the blue radial convergence coil is adjusted by R_9. As the blue convergence requires a predominantly parabolic current, additional integration is required, and is provided by C_6. The waveform produced by this method of integration is basically sinusoidal, however, and it requires further modification that is obtained by adding a second-harmonic sinusoidal waveform from a resonant circuit consisting of C_5 and the adjustable blue shape control inductor L_{16}. The amplitude of current flowing through this shaping network is controlled by the blue tilt control R_{15}.

When a high degree of overall convergence is required some dynamic blue lateral correction is essential. The coils on the blue lateral convergence assembly are provided for this purpose and are connected into the deflector coil circuit. Since either phase of the correction waveform may be required, provision for reversing the connections to the blue lateral coils should be arranged. The current flowing through the blue lateral coils is controlled by a variable shunt inductor L_{15} which has alternative taps to increase the range of current control if required.

All the potentiometers and variable resistors are wirewound types. Taking into account the dissipation of the resistors at various settings, it is suggested that these ratings should be 2W for R_{10}, R_{12}, and R_{14}, and 4W for R_9 and R_{15}.

DYNAMIC FIELD CONVERGENCE

The output from a valve or transistor field output stage can be used for dynamic field convergence.

Valve Deflection Circuit

The waveform available at the cathode of the field output valve may be used for dynamic field convergence. However, the introduction of the field convergence circuit may cause degeneration in the timebase which will result in a non-linear field scan at the bottom of the screen. Such effects can be minimised by connecting the convergence coils in parallel to produce a lower impedance circuit.

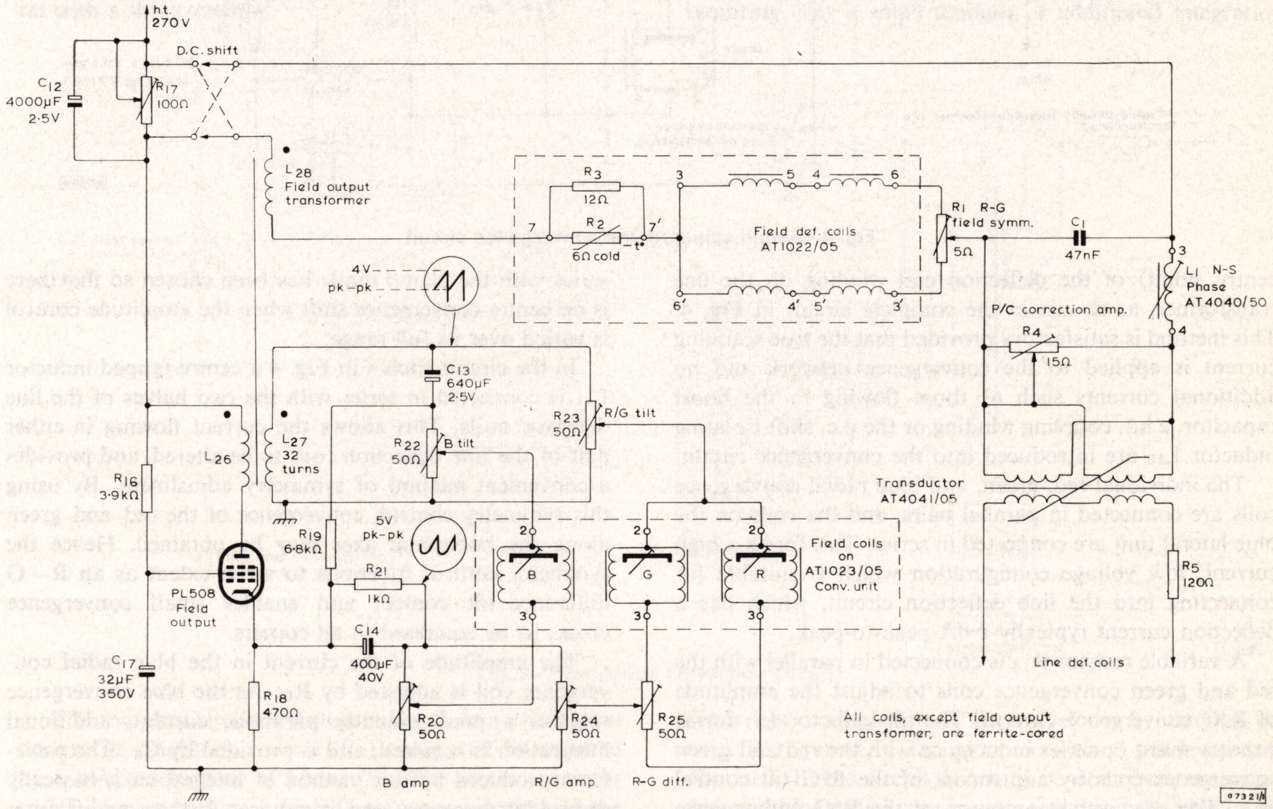
h.t.
270V
D.C. shift
C12
4000µF
2·5V
R17
100Ω
L28
Field output
transformer
R3
12Ω
R2
6Ω cold
7
7'
t°
3
5
4
6
6'
4'
5'
Field def. coils
AT1022/05
R1 R-G
field symm.
5Ω
C1
47nF
L1 N-S
Phase
AT4040/50
P/C correction amp.
R4
15Ω
4V
pk-pk
C13
640µF
2·5V
R23
50Ω
R/G tilt
R22
50Ω
B tilt
L27
32
turns
L26
R16
3·9kΩ
Transductor
AT4041/05
5V
pk-pk
R19
6·8kΩ
R21
1kΩ
PL508
Field
output
B
G
R
2
3
Field coils
on
AT1023/05
Conv. unit
R5
120Ω
Line def. coils
C14
400µF
40V
C17
32µF
350V
R18
470Ω
R20
50Ω
R24
50Ω
R25
50Ω
B amp
R/G amp
R-G diff.
All coils, except field output
transformer, are ferrite-cored
a7321

Fig. 5—Field dynamic convergence circuit for use with valve field timebase

A complete circuit is shown in Fig. 5. A combined sawtooth plus parabolic waveform is supplied from the cathode of the field output valve to the convergence coils via the amplitude controls R_{20} and R_{24}. An opposing sawtooth waveform is taken from a 32-turn winding (L_{27}) on the field output transformer and is applied to the convergence coils via the tilt controls R_{22} and R_{23}. This additional antiphase waveform enables the sawtooth component in the convergence coils to be varied. A d.c. component is added to the convergence waveforms by R_{19} and R_{21} to reduce or eliminate the need for readjustment of the static convergence magnets during and after convergence.

A field symmetry control is provided by means of a potentiometer R_1 which is connected in series with the two pairs of field deflection coils. This adjustment is used in conjunction with the field convergence R−G difference control R_{25} to converge the red and green horizontal lines at the top and bottom of the picture.

Transistor Deflection Circuit

When transistors are used in the field output stage and the single ended push-pull configuration is employed, the field output valve and the associated transformer are eliminated (Ref. 2). Hence other waveform sources are required to supply the field dynamic convergence coils. Satisfactory field dynamic convergence can be obtained if the current flowing in the field deflector coils is used as a waveform source. This current can be sampled across a series connected resistor, and the resulting waveform supplied to the field convergence coils through suitable shaping networks. The complete circuit is shown in Fig. 6.

The scanning waveform is sampled across R_{24} which forms the R/G amplitude control and is applied to the red and green convergence coils. A parabolic waveform is developed across C_7 connected in series with the R/G tilt control R_{23}. Adjustment of the amplitude and tilt controls therefore enables the amplitude of the sawtooth and parabolic waveforms in the coils to be varied. A clipping diode D_2 shapes the parabolic waveform developed across C_7 and also serves to clamp the centre R/G convergence.

The blue convergence coils require a sawtooth waveform with a differential component added. The waveform developed across the series resistor is therefore differentiated by C_8 and R_{20} (the blue amplitude control). Variation of the sawtooth component is simply achieved by shunting the capacitor with a variable resistor R_{22} (the blue tilt control).

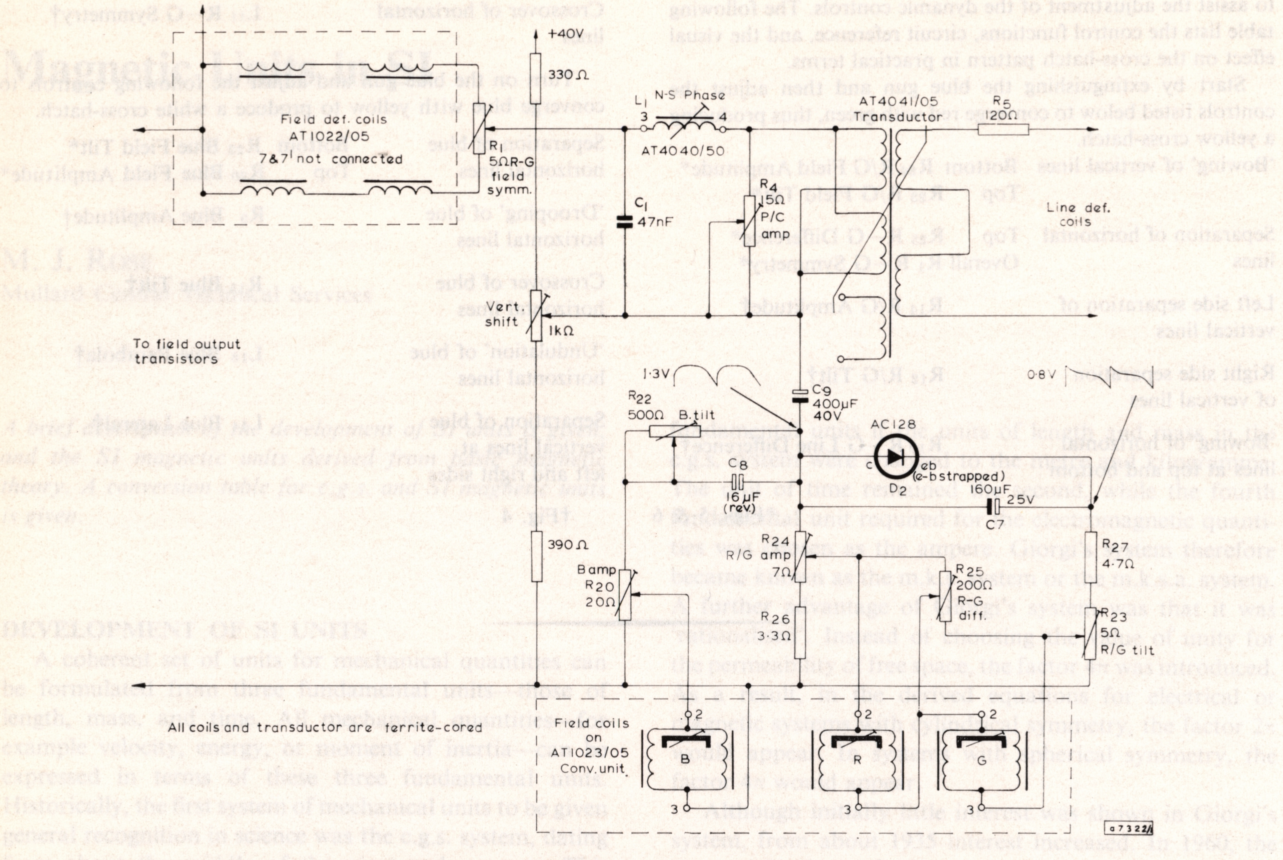
+40V
330Ω
Field def. coils
AT1022/05
7&7' not connected
R1
5ΩR-G
field
symm.
L1 N-S Phase
3
4
AT4040/50
AT4041/05
Transductor
R5
120Ω
C1
47nF
R4
15Ω
P/C
amp
Line def.
coils
Vert.
shift
1kΩ
To field output
transistors
1·3V
R22
500Ω
B.tilt
C9
400µF
40V
AC128
c
eb
(e-b strapped)
D2
C8
16µF
(rev)
160µF
25V
C7
390Ω
R24
R/G amp
7Ω
R27
4·7Ω
B amp
R20
20Ω
R25
200Ω
R-G
diff.
R26
3·3Ω
R23
5Ω
R/G tilt
0·8V
All coils and transductor are ferrite-cored
Field coils
on
AT1023/05
Conv. unit
B
R
G
2
3
a7322

Fig. 6—Pincushion correction and convergence circuit for use with transistor field timebase

Capacitor C_8 should be a reversible electrolytic type, and the tolerance for both C_7 and C_8 should be not more than ±20%. It is also important that the capacitors have a low series resistance.

REFERENCES

1. 'Colour Television: a background to colour tube adjustments for the service engineer'. Mullard Limited, 1968, TP1020.
2. Attwood, B. E., 'Transistor Field Timebases for Colour and Monochrome Receivers'. **Mullard Technical Communications**, Vol. 9, No. 89, Sept. 1967, pp. 246 to 251.

APPENDIX

CONVERGENCE PROCEDURE

Static Convergence

The object of static convergence is to cause the three individual beams to be superimposed in the centre of the screen. This is achieved by the use of three disc magnets mounted symmetrically 120° apart on the radial convergence yoke with their fields directed into the convergence pole-piece of each electron gun.

As the red and green magnets are located at angles of 120° and 240° respectively they will move the red and green beams along the 120° and 240° radial axes. By adjusting these magnets the red and green beams can be superimposed at the centre of the screen.

To enable the blue beam also to be superimposed at this point, both horizontal and vertical movement of this beam will be required. The blue radial static magnet is mounted vertically above the blue pole-piece, and rotating it causes the blue beam to move up and down along a vertical axis. The horizontal movement is accomplished by means of a blue lateral convergence magnet which directs the field from two rod magnets, mounted near the base of the picture tube, into the blue gun. The adjustment of the blue radial and lateral magnets until the blue beam coincides with the convergent red and green beams completes the static convergence procedure. An illustrated account of the setting-up procedure is given in '*Colour Television*' (Ref. 1).

Dynamic Convergence

When the convergence of the three beams in the centre of the screen has been achieved, it is necessary to correct for the misconvergence caused by field and line deflection. Before commencing dynamic convergence, it is essential that the receiver should have been degaussed and the width, line linearity, height, field linearity and purity adjusted.

It is normal practice to display a white cross-hatch pattern to assist the adjustment of the dynamic controls. The following table lists the control functions, circuit reference, and the visual effect on the cross-hatch pattern in practical terms.

Start by extinguishing the blue gun and then adjust the controls listed below to converge red with green, thus producing a yellow cross-hatch.

'Bowing' of vertical lines	Bottom	R_{24} R/G Field Amplitude*
	Top	R_{23} R/G Field Tilt*
Separation of horizontal lines	Top	R_{25} R−G Difference*
	Overall	R_1 R−G Symmetry*
Left side separation of vertical lines		R_{14} R/G Amplitude†
Right side separation of vertical lines		R_{12} R/G Tilt†
'Bowing' of horizontal lines at top and bottom		R_{10} R−G Line Difference†
Crossover of horizontal lines		L_{11} R−G Symmetry†

Turn on the blue gun and adjust the following controls to converge blue with yellow to produce a white cross-hatch.

Separation of blue horizontal lines	Bottom	R_{22} Blue Field Tilt*
	Top	R_{20} Blue Field Amplitude*
'Drooping' of blue horizontal lines		R_9 Blue Amplitude†
Crossover of blue horizontal lines		R_{15} Blue Tilt†
'Undulation' of blue horizontal lines		L_{16} Blue Parabola†
Separation of blue vertical lines at left and right sides		L_{14} Blue Lateral†

*Figs. 5 & 6

†Fig. 4

Magnetic Units in SI

M. J. Rose
Mullard Central Technical Services

A brief description of the development of SI units is given, and the SI magnetic units derived from basic magnetic theory. A conversion table for c.g.s. and SI magnetic units is given.

DEVELOPMENT OF SI UNITS

A coherent set of units for mechanical quantities can be formulated from three fundamental units—those of length, mass, and time. All mechanical quantities—for example velocity, energy, or moment of inertia—can be expressed in terms of these three fundamental units. Historically, the first system of mechanical units to be given general recognition in science was the c.g.s. system, dating from about the middle of the nineteenth century. This system used the centimetre, gramme, and second as the fundamental units.

Complications arose when the c.g.s. system was applied to electrical and magnetic phenomena. At least one other fundamental unit was required to define electrical or magnetic quantities, and in fact two parallel systems were developed. These were the c.g.s. electrostatic system, and the c.g.s. electromagnetic system.

In the c.g.s. electrostatic system, the observed inverse-square law of the force between two electrical charges can be used to define the basic unit of electrical charge in terms of a constant, the permittivity of free space. Similarly, the observed force between two magnetic poles enables the unit of magnetic pole strength to be defined in terms of the permeability of free space. Values of unity were given to both these constants.

Unfortunately the units for the same quantity derived from the two systems sometimes differed considerably. The unit of current, for example, in the electrostatic system—the statampere—is not the same as the unit of current in the electromagnetic system—the abampere. Also, the abampere of the electromagnetic system was too large a unit for practical purposes in current electricity, while the abvolt was far too small. Thus the abampere was multiplied by 10^{-1} to give the ampere, and the abvolt by 10^8 to give the volt. These units with corresponding ones such as the coulomb, ohm, and watt were incorporated with the c.g.s. mechanical units to give a third system, the practical system.

In 1904, G. L. T. Giorgi showed that the practical units of electromagnetism could be directly related to the fundamental units if the units of length and mass in the c.g.s. system were changed to the metre and kilogramme. The unit of time remained the second, while the fourth fundamental unit required for the electromagnetic quantities was chosen as the ampere. Giorgi's system therefore became known as the m.k.s. system or the m.k.s.a. system. A further advantage of Giorgi's system was that it was 'rationalised'. Instead of choosing the value of unity for the permeability of free space, the factor 4π was introduced. As a result, in the derived equations for electrical or magnetic systems with cylindrical symmetry, the factor 2π would appear. In systems with spherical symmetry, the factor 4π would appear.

Although initially little interest was shown in Giorgi's system, from about 1935 interest increased. In 1960, the General Conference of Weights and Measures incorporated the m.k.s. system into a comprehensive system of units known as the Système International d'Unités (SI). SI is now the standard system throughout science and technology wherever metric units are employed. There are six fundamental units. Besides the metre, kilogramme, second, and ampere already mentioned, the other two fundamental units are the kelvin for thermodynamic quantities, and the candela for photometry.

CLASSICAL ISOLATED-POLE MAGNETIC THEORY

Before considering the SI magnetic units, a brief resumé of the derivation of the main magnetic quantities will be given. A convenient starting point for the development of the classical magnetic theory is the observed force between two magnetic poles.

Although an isolated magnetic pole cannot exist, an approximation can be achieved by using long magnets of small diameter. Experiments with such magnets showed that the force between two magnetic poles was dependent on:

the magnitude and polarity of the magnetic poles,
the magnetic property of the medium separating them,
the square of the distance between them.

This relationship may be expressed mathematically as:

$$F \propto \frac{m_1 \cdot m_2}{x^2},$$

where m_1 and m_2 represent the magnitude and polarity of the two poles, and x the distance between them. This is the well-known inverse-square law.

If the two poles m_1 and m_2 have equal strengths, and the constant of proportionality is made unity, the pole strength can be expressed in terms of unit force and unit distance. Thus in the c.g.s. system, unit pole strength was defined as the pole strength which when placed 1cm from a similar pole would produce a force of one dyne.

In SI, the equation for the force between two magnetic poles can be written:

$$F = \frac{m_1 \cdot m_2}{4\pi\mu x^2}, \qquad \ldots(1)$$

where μ is the magnetic permeability of the medium separating the poles.

The magnetic field strength at a point is defined as the force acting upon unit pole at that point. Thus the magnetic field strength H can be derived from Eq.1 by making m_2 unity and generalising to give:

$$H = \frac{m}{4\pi\mu x^2}, \qquad \ldots(2)$$

where x is the distance between the pole m producing the magnetic field and the point at which the field strength is being measured.

An isolated magnetic pole m produces a magnetic flux Φ emanating in all directions, and equal in value to m in all media. Thus:

$$\Phi = m. \qquad \ldots(3)$$

The flux density B at a point distant x from a pole m is the flux per unit (normal) area, that is:

$$B = \frac{\text{flux}}{\text{surface area of sphere of radius x}},$$

and from Eq.3:

$$B = \frac{m}{4\pi x^2}. \qquad \ldots(4)$$

If the field strength and flux density at the same point are compared, then from Eqs.2 and 4:

$$B = \frac{m}{4\pi x^2},$$

$$H = \frac{m}{4\pi\mu x^2} = \frac{B}{\mu}.$$

Thus:

$$\mu = \frac{B}{H}. \qquad \ldots(5)$$

SI MAGNETIC UNITS

From the preceding section it can be seen that the main magnetic units are:

field strength H,
flux Φ,
flux density B,
permeability μ.

The unit of **field strength** (the oersted of the c.g.s. system) is **ampere per metre.**

The unit of **flux** (the c.g.s. maxwell or lines) is the **weber.**

The unit of **flux density** (the c.g.s. gauss) is weber per square metre or **tesla.**

The unit of **permeability is henry per metre.**

The conversion factors for these SI and c.g.s. units are listed in the table.

Another magnetic quantity that is commonly used is the BH product which is a measure of the magnetic energy available at a particular working point. The c.g.s. unit for this quantity was the gauss-oersted, and the SI unit is the tesla-ampere per metre.

UNITS OF FIELD STRENGTH AND PERMEABILITY

At first sight it may seem strange that the unit of magnetic field strength is ampere per metre, and that for permeability henry per metre. The way that these units are obtained will be shown below.

Unit of Field Strength

An infinitely long straight conductor carrying a current I amperes is shown in Fig. 1. The magnetic field strength at a point P produced by an element $\delta\ell$ of the conductor will be considered. The point P is at a distance x metres and angle θ from the element, and r metres normally from the conductor.

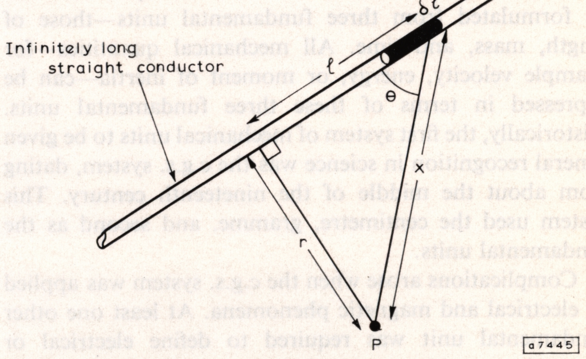

Fig. 1—Configuration for calculating magnetic field strength produced by infinitely long straight conductor

The magnetic field strength at P due to the element $\delta\ell$ is:

$$\delta H = \frac{I\delta\ell\sin\theta}{4\pi x^2}. \qquad \ldots(6)$$

From the geometry of the configuration in Fig. 1, it can be seen that:

$$x = r.\text{cosec}\theta;$$

and:

$$\frac{\ell}{r} = \cot\theta,$$

which on differentiation gives:

$$\delta\ell = -r.\text{cosec}^2\theta\delta\theta.$$

Thus Eq.6 can be written as:

$$\delta H = \frac{I(-r.\text{cosec}^2\theta.\sin\theta)\delta\theta}{4\pi r^2.\text{cosec}^2\theta},$$

so that the total field strength at P is:

$$H = \frac{I}{4\pi r}\int_{\pi}^{0} -\sin\theta d\theta.$$

Evaluating the integral gives:

$$H = \frac{I}{2\pi r}.$$

In this equation, the unit of I is the ampere, and that of r is the metre. Therefore the unit of magnetic field strength H is ampere per metre.

Unit of Permeability

The unit of permeability can be derived by considering the inductance of a closed magnetic circuit such as the toroidal coil shown in Fig.2. The core has a cross-sectional area of A square metres, and the coil has n turns.

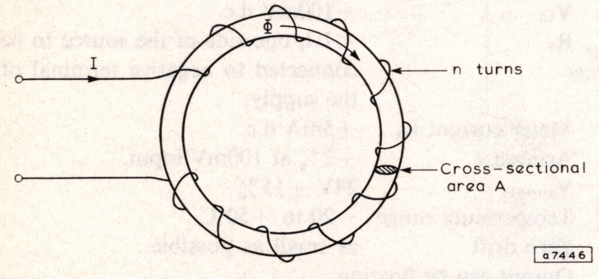

Fig. 2—Toroidal coil

If a current I amperes through the coil produces a flux Φ webers, the inductance L of the coil (defined as the number of flux linkages per unit current) is:

$$L = \frac{n\Phi}{I}. \qquad \ldots(7)$$

The flux density in the core is Φ/A tesla, and so the general relationship $B = \mu H$ can be rewritten as:

$$\mu = \frac{\Phi/A}{H}. \qquad \ldots(8)$$

But Φ can be obtained in terms of the inductance of the circuit from Eq.7, giving:

$$\Phi = \frac{LI}{n},$$

so that Eq.8 becomes:

$$\mu = \frac{LI/nA}{H} = \frac{LI}{nAH}.$$

The units of all these quantities are known; therefore:

$$\text{unit of } \mu = \frac{(\text{unit of inductance}=\text{henry})\times\text{ampere}}{\text{metre}^2\times\text{ampere per metre}},$$

since n (the number of turns in the coil) is dimensionless. Therefore the unit of permeability is henry per metre.

NOTE

The object of this article has been to introduce the SI magnetic units in a simple manner. More rigorous mathematical treatments are possible, of course, based usually on the fundamental definition of the ampere through the force between two straight infinitely long current-carrying conductors. Such treatments will be found in most modern textbooks on electromagnetic theory.

BIBLIOGRAPHY

British Standard 3763: 1964 **The International System (SI) Units.** British Standards Institution, 1964. (Defines the six basic SI units and the important derived units)

The Use of SI Units. British Standards Institution, 1967.

JERRARD, H.G. and MCNEILL, B. D., **A Dictionary of Scientific Units,** Science Paperbacks and Chapman & Hall Ltd, London, 1966.

ANDERTON, P. and BIGG, P. H., **Changing to the Metric System,** HMSO, Second edition, London, 1967.

SI and C.G.S. Magnetic Units with Conversion Factors

Quantity	SI unit	C.G.S. unit	Conversion factor*
Magnetic field strength	ampere per metre (A/m)	oersted	$10^3/4\pi$
Magnetic flux	weber (Wb)	maxwell or line	10^{-8}
Magnetic flux density	tesla (T)	gauss	10^{-4}
Permeability	henry per metre (H/m)	—	$4\pi\times10^{-7}$
Magnetic energy (BH product)	tesla-ampere per metre (T A/m)	gauss-oersted	$1/(40\pi)$

*Conversion factor to multiply c.g.s. unit with to obtain corresponding SI unit

D.C. Amplifier to drive an Electrolytic Ampere-hour Meter

R. S. Babbs
Mullard Central Application Laboratory

A transistor pair is used in a long-tailed pair amplifier to drive an electrolytic A-h meter. Dynamic loads are provided by transistors, and negative feedback is applied to control the mean collector voltage of the amplifier transistors. A simple supply voltage stabiliser is incorporated.

The meter current is 5mA for an input voltage of 100mV. The drift is small.

INTRODUCTION

This article describes an amplifier which converts a d.c. signal of up to ±100mV from a low source resistance into a directly proportional current of up to ±5mA to be passed through an electrolytic ampere-hour meter.

Essentially, the amplifier is required to operate from a 24V ±15% supply, have low drift with time and temperature, and be cheap. One terminal of the source is to be common with the negative terminal of the power supply.

These requirements have been met with a simple circuit. This article gives details of the load, and describes the requirements, design, and performance of the amplifier.

DESCRIPTION OF THE LOAD

The load is an electrolytic cell consisting of a length of precision bore glass tube having an electrode sealed in at each end and containing two columns of mercury separated by a small gap filled with an aqueous electrolyte. When a current is passed through the cell, mercury is transferred across the gap from one column to the other. Thus the gap moves along the tube (in the opposite direction to the transfer of the mercury) at a rate proportional to the current. The amount of gap travel, which can be observed visually against an adjacent scale, is a precise measure of the total quantity of electricity passed through the cell. Thus it acts as a coulombmeter (or A-h meter) and gives an accurate indication of the time integral of the current passed through it in either direction; or, if operated at a constant current, acts as an elapsed time meter.

One of the characteristics of this type of cell is that its resistance doubles for every decade decrease of current. A typical maximum current is 5mA, and resistance at that current at 20°C is 110Ω. Thus at 1μA the resistance is 1·8kΩ. With fall in temperature, the resistance rises at the rate of roughly 1·1%/degC.

REQUIREMENTS

The specification which the amplifier is required to meet is set out below.

V_{in}	±100mV d.c.
R_s	<1Ω, one side of the source to be connected to negative terminal of the supply.
Meter current I_m	±5mA d.c.
Accuracy	±2% at 100mV input.
V_{supply}	24V ±15%
Temperature range	−20 to +50°C
Zero drift	as small as possible
Output can be floating	
Component cost as low as possible.	

DESCRIPTION OF THE AMPLIFIER

Fig. 1 shows the circuit diagram of the directly-coupled amplifier and supply voltage stabiliser. The amplifier consists basically of a differential amplifier having two transistors TR_{1a} and TR_{1b} in a long-tailed pair circuit with the A-h meter connected between the two collectors. A matched pair of transistors (a BCY89) is used to obtain low drift, small shift of zero with input signal, and good power supply rejection. Even so, the power supply variation of ±3·6V is considered too large, and a simple stabiliser TR_5 (described later) is incorporated. This gives a nominal 17·4V supply, and the amplifier is designed to operate from this.

The signal voltage V_{in}, developed across the source resistance R_s, is applied to the bases of TR_{1a} and TR_{1b} via potential dividers R_1, R_2 and R_{12}, R_{13}, R_{14}. The attenuation of the signal by these potential dividers is made as small as possible by choosing the value of R_2 and R_{14} small compared to that of R_1 and R_{12}. The minimum ratio is governed by the sum of the V_{be} of TR_1, the voltage drop across the emitter resistors R_4 and R_6, and the V_{ce} of TR_2, a total of 1·9V.

In order that the variation of A-h meter resistance with current shall have little effect on the performance, the output resistance of the amplifier needs to be high compared with the maximum resistance of the A-h meter. This means a high value of impedance between the collector of each amplifier transistor and the positive supply. As this cannot be provided by a resistor, because the d.c. voltage drop will be too high, a p-n-p transistor (TR_3, TR_4) is used in the common emitter configuration to present a high dynamic resistance to the collector of each amplifier transistor, but having a low d.c. voltage drop. The current through these p-n-p transistors is controlled by the common base voltage divider R_{10}, R_{11} and the two emitter resistors R_3 and R_9.

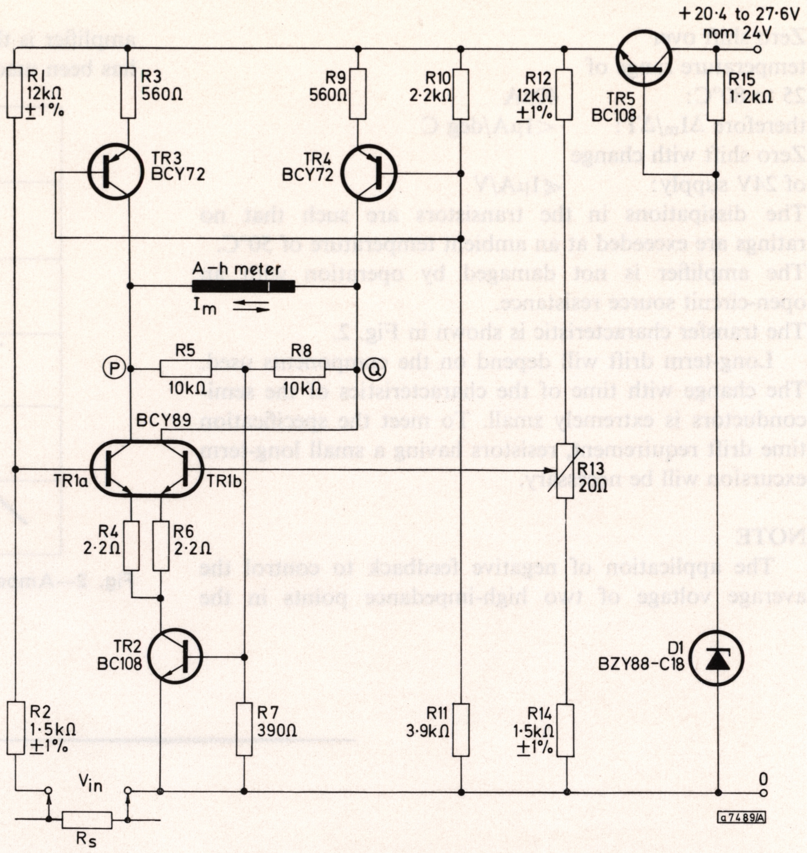

Fig. 1—Drive circuit for ampere-hour meter. All resistor values ±5% unless otherwise specified

The problem of stabilising the voltage at points P and Q (the joins of the collectors of TR_{1a} and TR_3 and TR_{1b} and TR_4 respectively) which is created by the use of the dynamic loads, is solved by applying common mode negative feedback from P and Q, via the two resistors R_5 and R_8, to the base of TR_2. This transistor forms the constant current source for the sum of the emitter currents of the amplifier transistors TR_{1a} and TR_{1b}. Because the voltage at the junction of R_5 and R_8 is proportional to the mean value of the potentials at the points P and Q, this feedback arrangement controls the average voltage, but has no effect on the differential action of the amplifier circuit.

With the component values shown, the collector voltages of TR_{1a} and TR_{1b} are 10V, their collector currents are 9·5mA, and the transconductance is the required 50mA/V.

Zero setting is provided by R_{13}, adjustment of which sets the current through the A-h meter to zero for zero input voltage.

Supply Voltage Stabiliser

The supply voltage stabiliser consists of an emitter follower TR_5, connected in series with the supply and with its base voltage controlled by a voltage regulator diode D_1. The diode is connected to the 24V supply by the resistor R_{15}.

The total current taken by the amplifier is 26mA. If TR_5 has a minimum current gain of 100, its base current is 260μA. Thus the current through D_1 can be easily made larger than this without becoming excessive when the supply voltage is at its highest value. With an 18V diode the voltage drop across R_{15} changes from 2·4V to 9·6V (a 4 to 1 ratio) over the full range of supply voltage. Hence if the minimum current through D_1 is made 2mA, its maximum value is 8mA, and R_{15} then becomes 1·2kΩ.

The maximum R_z of the BZY88-C18 is 50Ω, so the maximum change of diode voltage with supply voltage is 300mV, and the stabiliser output voltage changes by very nearly the same amount. The change of diode voltage with temperature is +15mV/degC and the change of the V_{be} of TR_5 is −2mV/degC leaving a net change of 13mV/degC. Over the temperature range of −20 to +50°C the change of output voltage for a constant supply voltage is 910mV. Both these variations are acceptable.

PERFORMANCE

The measured performance of the amplifier to drive the A-h meter is summarised below.

Transconductance: (The change of this conductance with temperature is negligible)	50mA/V
Zero shift:	
2s after removal of signal that gives full meter current:	<5μA
10s after:	<0·5μA

Zero shift over
temperature range of
25 to 80°C: $40\mu A$
therefore $\Delta I_m/\Delta T$: $<1\mu A$/deg C
Zero shift with change
of 24V supply: $\leqslant 1\mu A/V$

The dissipations in the transistors are such that no ratings are exceeded at an ambient temperature of 50°C.

The amplifier is not damaged by operation with an open-circuit source resistance.

The transfer characteristic is shown in Fig. 2.

Long-term drift will depend on the components used. The change with time of the characteristics of the semiconductors is extremely small. To meet the specification time drift requirement, resistors having a small long-term excursion will be necessary.

NOTE

The application of negative feedback to control the average voltage of two high-impedance points in the amplifier is thought to be novel, and a patent application has been made.

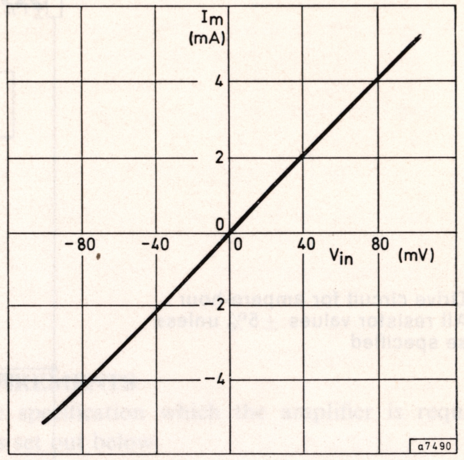

Fig. 2—Ampere-hour meter current as a function of input voltage (measured curve)